Eur. Phys. J. B **38**, 501–513 (2004)
DOI: 10.1140/epjb/e2004-00145-6

THE EUROPEAN PHYSICAL JOURNAL B

Josephson effect between superconducting nanograins with discrete energy levels

D. Gobert[a], U. Schollwöck, and J. von Delft

Sektion Physik and CeNS, Ludwigs-Maximilians-Universität München, Theresienstr. 37, 80333 München, Germany

Received 2 May 2003 / Received in final form 8 September 2003
Published online 28 May 2004 –

Abstract. We investigate the Josephson effect between two coupled superconductors, coupled by the tunneling of pairs of electrons, in the regime that their energy level spacing is comparable to the bulk superconducting gap, but neglecting any charging effects. In this regime, BCS theory is not valid, and the notion of a superconducting order parameter with a well-defined phase is inapplicable. Using the density matrix renormalization group, we calculate the ground state of the two coupled superconductors and extract the Josephson energy. The Josephson energy is found to display a reentrant behavior (decrease followed by increase) as a function of increasing level spacing. For weak Josephson coupling, a tight-binding approximation is introduced, which illustrates the physical mechanism underlying this reentrance in a transparent way. The DMRG method is also applied to two strongly coupled superconductors and allows a detailed examination of the limits of validity of the tight-binding model.

PACS. 74.20.-z Theories and models of superconducting state – 74.78.-w Superconducting films and low-dimensional structures – 74.50.+r Tunneling phenomena; point contacts, weak links, Josephson effects

1 Introduction

The Josephson effect, i.e. the flow of a zero-voltage current between two weakly coupled superconductors, with a sign and amplitude that depends on the difference of the phases of their respective order parameter, can be regarded as one of the most striking illustrations of phase coherent behaviour in a macroscopic system and as one of the hallmarks of superconductivity. Although the Josephson effect is in general well understood, there is still a regime in which it has not yet been studied in detail: superconductors that are so small that the discrete nature of their energy levels becomes important. In this regime, the theory of Bardeen, Cooper and Schrieffer (BCS), which the quantitative understanding of the Josephson effect has been based on, is not applicable. This is because BCS theory relies on the assumption of a continuous energy band, and is not consistent once the level spacing exceeds the superconducting gap Δ_{BCS} [1,2].

When it became possible to reach this regime experimentally by doing transport measurements on superconducting grains with a diameter of only a few nanometers [2,3], interest was spurred in a description of the pair-correlated state that is also valid for $d > \Delta_{\mathrm{BCS}}$. The rediscovery of an exact solution of the BCS Hamiltonian with discrete levels, found in 1964 by Richardson [4], allowed to explore in detail the breakdown of BCS theory as d increases. Several surprising insights were gained, one of which being that BCS theory already becomes unreliable when $d \geq \Delta_{\mathrm{BCS}}^2/\omega_{\mathrm{Debye}}$, in other words, long before the criterion $\Delta_{\mathrm{BCS}} \sim d$ is met [5].

Another issue that arises for small superconductors is that the superconducting phase ϕ is not well-defined: When the mean number of electron pairs $\langle N \rangle$ is so small that fluctuations around $\langle N \rangle$ in the grand canonical ensemble are not negligible anymore, N has to be treated as fixed. As a consequence, due to the uncertainty relation $[N, \phi] = i$, the notion of an order parameter with a well-defined phase loses its meaning.

Therefore, a very natural question arises: What is the fate of the Josephson effect between two small superconducting grains, in a regime where BCS theory breaks down, and where the notion of a superconducting phase variable is no longer valid?

In this paper, we examine this question in detail by studying two pair-correlated grains, coupled by a tunneling term that allows pairs of electrons to tunnel between the grains. We study this system using the density-matrix renormalization group (DMRG), a powerful numerical approach applicable to strongly correlated systems, which has already proven to be useful for calculating the properties of single superconducting grains [7,18]. We here use it to calculate the ground state of two coupled grains and to extract the Josephson energy. For weak Josephson

[a] e-mail: gobert@lmu.de

coupling, we also perform a tight-binding approximation and compare its results to those of the DMRG calculation for two coupled grains.

We identify two competing effects due to the discreteness of the energy levels: Somewhat surprisingly, the Josephson energy is found to be enhanced for large level spacing due to the contribution of a single energy level. At intermediate level spacing, a kinetic energy term dominates, which suppresses the Josephson energy. The competition of these effects leads to a surprising reentrant behavior (decrease followed by increase) of the Josephson energy as a function of increasing level spacing. In the limit of vanishing level spacing, the BCS result is recovered.

At this point, we should mention an important restriction on our analysis: In the regime of small superconductors that we are interested in, the charging energy for an electron pair to tunnel between the two superconductors can become huge, easily of the order of a few hundred Kelvin in the experiments of [2]. As will be explained in some detail in Section 2.4, the dominant effect of the charging energy is to suppress tunneling events altogether and thereby to destroy the Josephson effect. However, the interest of the present paper is to study the effects due to the discrete spacing of the energy levels rather than that of charging effects, which have been thoroughly examined already [11,12,15]. Therefore, we set the charging energy to zero in this paper.

To experimentally realize the no-charging-energy model studied here, one needs systems for which the mean level spacing is larger than the charging energy. In principle, it is possible to reduce the charging energy of isolated grains, e.g. by using a pancake-shaped grain geometry in order to increase the inter-grain capacitance area, or by embedding the grains in a strong dielectric medium. — A more radical and at this point purely speculative way of studying Josephson physics in the absence of charging effects would be to use uncharged particles instead of electrons, e.g. a degenerate Fermi gas of charge-neutral cold atoms in a double-well trapping potential. As for now, low enough tempertatures for observing a "superconducting" phase of cold neutral fermionic atoms were not yet obtained, but are predicted to be within reach [10]. Once this has been achieved, a natural next step would be to study the Josephson effect in this system, for which the charging energy would indeed be zero, but the level spacing finite due to the spatial confinement in the trapping potential. Then, the present discussion of the Josephson effect in the presence of finite level spacing should be very relevant.

The outline of the paper is as follows: In Section 2, we review the theory of the Josephson effect in a way that is also applicable for small superconductors, for which standard BCS theory is not applicable, and we give a definition of the Josephson energy independently of a superconducting phase variable. Section 3 contains a brief introduction to the DMRG method and its application to the system of two coupled superconductors. Finally, in Section 4 we present and discuss the results of our calculation.

2 Josephson effect for weakly coupled superconductors: Theory

In this section, we review some standard results of the theory of the Josephson effect and explain their relation to the pair-tunneling models to be used below. Our discussion of the Josephson effect is restricted to weak coupling between superconductors, such that perturbation theory in the coupling can be applied. We are careful, however, to formulate the Josephson effect in such a way that a generalization beyond perturbation theory is possible; this is done in the last Section 2.6.

The physical assumption underlying perturbation theory is that the tunnel coupling between the superconductors is so weak that it is energetically not favorable to create excited states with broken electron pairs in the individual grains. Therefore, the low-energy states of the coupled system will not contain any of these excitations, which will only be present as virtual states in perturbation theory. In more quantitative terms, the weak-coupling condition is $E_J^0 \ll \Delta_{\rm sp}$, where $\Delta_{\rm sp}$ is the lowest energy of a pair-breaking excitation, and the Josephson tunneling matrix element E_J^0 is defined in equation (15) below.

We are also careful to formulate our discussion of the Josephson effect independently of the notion of a superconducting phase variable, such that it remains valid in the regime of small superconductors. The material in this section is mostly not new and has been discussed in one way or the other previously [6,8], but we feel it is worth presenting it in a way that makes the ensuing application to small grains evident.

2.1 Josephson effect as a phase dependent delocalization energy

In the grand canonical ensemble, the phase of a superconductor ϕ can be defined via the action of the pair annihilation operator [21] $b_i = c_{i\uparrow}c_{i\downarrow}$, and the state $\big|\phi\rangle$ is said to have a phase ϕ if

$$\langle\phi\big|b_i\big|\phi\rangle \sim e^{i\phi}, \tag{1}$$

ϕ being independent of the state i (this is the case for the ground state of a superconductor). A familiar example is the well-known BCS ansatz wave function $\big|\phi\rangle = \prod_i (u_i + v_i e^{i\phi} b_i^\dagger)\big|0\rangle$, where u_i and v_i are real. Equation (1) implies that a state with definite phase ϕ must be a superposition of many states $\big|N\rangle$, each of which has a fixed number N of electron pairs:

$$\big|\phi\rangle = \sum_{N\geq 0} C_N \mathrm{e}^{iN\phi}\big|N\rangle, \tag{2}$$

subject to the condition that $\langle N\big|b_i\big|N+1\rangle$ is real, and with real coefficients C_N.

In the canonical ensemble, however, where the number of electron pairs N is fixed, the expectation value (1) vanishes, and the notion of a superconducting phase ϕ is obviously not valid. Nevertheless, the concept of a phase

difference φ between two coupled superconductors ("left" and "right", say) is still applicable, because the number of electron pairs on each individual superconductor need not be definite as long as the total number on both superconductors is fixed. In analogy to equation (1), φ can, then, be defined as

$$\langle\varphi|b_r b_l^\dagger|\varphi\rangle \sim e^{i\varphi}. \tag{3}$$

Here, the operators b_l and b_r refer to energy levels l, r of the left and right superconductors, respectively. As in equation (1), one has to assume that the phase in equation (3) is independent of the levels l and r for φ to be well-defined.

An example of a state with definite phase difference φ is, in analogy to equation (2),

$$|\varphi\rangle = \sum_{\nu=-N/2}^{N/2} C_\nu e^{i\nu\varphi}|\nu\rangle. \tag{4}$$

with real coefficients C_ν. Here, the states $|\nu\rangle$ denotes arbitrary states with $N/2-\nu$ pairs on the left and $N/2+\nu$ pairs on the right superconductor, subject to the condition that $\langle\nu|b_r b_l^\dagger|\nu+1\rangle$ is real.

We will be only interested in situations for which $|\nu\rangle$ has the form

$$|\nu\rangle = |N/2-\nu\rangle_L \otimes |N/2+\nu\rangle_R, \tag{5}$$

where $|n\rangle_{L,R}$ are the superconducting ground states of the isolated L- ("left") or R- ("right") superconductors, each containing a definite number of pairs, n. These states can always be chosen to satisfy the above reality condition.

As was pointed out by Josephson, the presence of a phase difference φ as in equation (3) has observable consequences when two superconductors are coupled: In particular, for weak coupling the coherent tunneling of pairs induces a zero-voltage current,

$$I = I_J \sin\varphi, \tag{6}$$

that explicitly depends on φ. As is well known [6,19], the Josephson current can, via the relation

$$I = (2e/\hbar)\partial E/\partial(\varphi), \tag{7}$$

also be interpreted as a dependence of the total energy E on the phase difference φ. For example, we expect equation (6) to follow from the energy-phase relation

$$E(\varphi) = \text{const.} - E_J\cos\varphi, \quad E_J = (\hbar/2e)I_J \tag{8}$$

which we will derive explicitly in Section 2.4 in the limit $d \to 0$. A more general definition of E_J, consistent with equation (8), will be given in Section 2.6, where we associate E_J with the energy gain in the ground state (i.e. $\varphi = 0$) due to the coherent tunneling of electron pairs.

The Josephson energy E_J sets the energy scale relevant for the Josephson effect: It is a delocalization energy that characterizes the coupling of two materials, their tendency to have the same phase and the maximum supercurrent $I_J = (2e/\hbar)E_J$ that can flow between them.

2.2 Pair tunneling Hamiltonian

Only processes that depend on the relative phase φ are relevant for the Josephson effect, as is illustrated in equation (7). Because of equation (3), such processes require the coherent tunneling of electron pairs; therefore, they have to be treated at least in second order in the tunneling of single electrons. The main goal of this subsection will be to derive an effective pair-tunneling Hamiltonian, equation (13) below, that arises at this order.

Consider two superconductors L and R (left and right), each having equally spaced energy levels with level spacing d, and each with a reduced BCS interaction with (dimensionless) coupling constant λ:

$$H_L = \sum_{l\sigma} \epsilon_l c_{l\sigma}^\dagger c_{l\sigma} - \lambda d \sum_{ll'} c_{l\downarrow}^\dagger c_{l\uparrow}^\dagger c_{l'\uparrow} c_{l'\downarrow}, \quad H_R \text{ similarly}, \tag{9}$$

where $\epsilon_l = l\,d$ is the bare energy of level l, $\sigma = \uparrow, \downarrow$ is the spin, and the sums are over all energy levels closer to the Fermi surface than the Debye energy ω_{Debye}.

Let L and R be coupled by single electron tunneling with constant tunneling matrix element t,

$$H_{1e} = -td \sum_{lr\sigma} c_{l\sigma}^\dagger c_{r\sigma} + \text{h.c.} \tag{10}$$

The coupling (10) lowers the total energy by generating states such as (4), that superimpose different numbers of electrons on each superconductor. For simplicity, we assume the sum in equation (10) to be cut off at ω_{Debye} in all numerical calculations below.

To second order in H_{1e}, the tunneling processes can be described by the effective tunneling Hamiltonian

$$H_2 = -\sum_{rl\sigma\nu} \frac{H_{1e}|rl\sigma\nu\rangle\langle rl\sigma\nu|H_{1e}}{E_{rl\nu}}, \tag{11}$$

acting on the space spanned by the states $|\nu\rangle$, defined in equation (5). The sum in equation (11) runs over all possible intermediate states $|rl\sigma\nu\rangle$ that can be reached by removing a single $(r\sigma)$-electron from state $|N/2-\nu\rangle_R$ and adding a single $(l\sigma)$-electron to state $|N/2+\nu\rangle_L$. $E_{rl\nu}$ is the corresponding excitation energy relative to the energy of the state $|\nu\rangle$. We assume, however, that for given r, l, σ, ν, all states except the one with the lowest energy give a negligibly small contribution to the sum, because of the following argument: In the BCS limit, which is valid for large enough values of λ, all excited states are described by the quasiparticle operators [19]

$$\gamma_{(e)\sigma i}^\dagger = u_i c_{i\sigma}^\dagger \mp v_i P^\dagger c_{i(-\sigma)}, \quad \gamma_{(h)\sigma i}^\dagger = u_i P c_{i\sigma}^\dagger \mp v_i c_{i(-\sigma)}, \tag{12}$$

where $P^\dagger$ is an operator that creates an additional pair. In this limit, it is easy to see that only the lowest energy state $|rl\sigma\nu\rangle = \gamma_{(e)\sigma l}^\dagger \gamma_{(h)(-\sigma)r}^\dagger |\nu\rangle$ gives a contribution to equation (11), whereas all other intermediate states have a vanishing overlap with $H_{1e}|\nu\rangle$. This is also the case for $\lambda = 0$, where $\gamma_{(e)\sigma l}^\dagger \gamma_{(h)(-\sigma)r}^\dagger = c_{\sigma l}^\dagger c_{\sigma r}$. For intermediate

values of λ, no simple argument can be made; we expect, however, that still the state with the lowest energy will give the dominant contribution.

The energy $E_{rl\nu}$ is given by the collective excitation energies $E_r + E_l$, arising from the fact that levels r and l are singly occupied. In general, it will also include a ν dependent contribution from charging energy due to the electron tunneling, see [15], but we chose to consider only situations in which these can be neglected.

In equation (11), two kinds of tunneling terms are present: on the one hand, terms proportional to $b_l^\dagger b_r$ or to $b_r^\dagger b_l$ that describe coherent pair tunneling, on the other hand, single electron terms proportional to $c_{r\sigma}c_{r\sigma}^\dagger c_{l-\sigma}^\dagger c_{l-\sigma}$ that describe the tunneling of a single electron from l to r and back. When the former terms are applied to a state $|\varphi\rangle$, defined in equation (4), they produce a phase dependent energy shift. In contrast, the latter terms only lead to a phase-independent energy shift, which is irrelevant for the Josephson effect. For this reason, the single electron terms can be omitted from the Hamiltonian (11), as long as only phase dependent processes are of interest [8]. Then, one finally arrives at the pair tunneling Hamiltonian

$$H_J = -2\sum_{rl} \frac{\gamma d^2}{E_r + E_l}(b_r^\dagger b_l + \text{h.c.}), \tag{13}$$

with $\gamma = t^2$. We shall use for the excitation energies their BCS values, $E_{r,l} = \sqrt{\Delta_{\text{BCS}}^2 + \epsilon_{r,l}^2}$.

2.3 Tight-binding model

In the space spanned by all states without any pair-breaking excitations, i.e. all states of the form $|\nu\rangle$ defined in equation (5), the Hamiltonian $H = H_L + H_R + H_J$ looks like a tight-binding Hamiltonian:

$$H = \begin{pmatrix} E(\nu) & -E_J^0/2 & 0 & \dots \\ -E_J^0/2 & E(\nu) & -E_J^0/2 & 0 \quad \dots \\ 0 & -E_J^0/2 & & \\ \vdots & 0 & & \\ & \vdots & & \end{pmatrix}, \tag{14}$$

where

$$E_J^0/2 = -\langle\nu|H_J|\nu+1\rangle, \tag{15}$$

$$E(\nu) = \langle\nu|(H_L + H_R)|\nu\rangle. \tag{16}$$

The ν dependence of the states $|N/2-\nu\rangle_L$ (and $|N/2+\nu\rangle_R$) occurring in equation (5) for $|\nu\rangle$ is very simple: All energy levels are shifted down (up) by an amount νd, assuming a constant level spacing d. Additionally, the ν empty levels closest to the upper cutoff are replaced by full levels at the lower cutoff (or vice versa). It is safe to assume that these levels do not influence the pairing correlations, as long as there are not extremely many of them, $\nu \ll N$, and as long as the coupling is not extremely large, $\lambda < 1$.

In this case, E_J^0 in equation (15) is independent of ν, and $E(\nu)$ in equation (16) is given by

$$E(\nu) = \text{const} + 2d(\nu - \nu_0)^2, \tag{17}$$

with ν_0 depending on gate voltage, i.e. on the shift of the single-particle energies ϵ_l and ϵ_r in equation (9) relative to each other. Equation (17) has the form of an effective charging energy term.

2.4 Discussion of the tight-binding model

In this subsection, we first discuss the above tight binding model (14) in the limit $d \to 0$ and check that it is consistent with the well-known result of Ambegaokar and Baratoff [9]. Then, we draw attention to what changes will occur as the superconductors become smaller.

In the bulk limit, $d \to 0$, the BCS ansatz can be applied. Within this approximation, the diagonal elements of H_J (17) are independent of ν, and the off-diagonal elements (15) are given by

$$E_J^0 = \sum_{lr} \frac{\Delta_{\text{BCS}}^2 t^2 d^2}{E_l E_r (E_l + E_r)} = \Delta_{\text{BCS}} t^2 \pi^2. \tag{18}$$

In the left equality of equation (18), the BCS expression for the matrix elements $\langle\nu|b_l\, b_r^\dagger|\nu+1\rangle = v_l u_l v_r u_r = \Delta_{\text{BCS}}^2/(2E_l E_r)$ has been used. For the right equality, the sum has been replaced by an integral, $\sum_{ij} = \int_{-\infty}^{\infty} \frac{d\epsilon_1\, d\epsilon_2}{d^2}$. No harm is done extending the integral range beyond ω_{Debye} to infinity, because it is naturally cut off at the scale Δ_{BCS} anyway, assumed to be much smaller than ω_{Debye}.

The energy eigenstates of (14) then have the form of equation (4) with constant coefficients C_ν. As anticipated in equation (8), they correspond to an energy $E(\varphi) = \text{const.} - E_J^0 \cos\varphi$, and therefore we can identify

$$E_J = E_J^0 = \Delta t^2 \pi^2 = \frac{\pi\hbar\Delta_{\text{BCS}}}{4e^2 R_N}. \tag{19}$$

The last equality expresses E_J in terms of the normal-state conductance $R_N^{-1} = (4\pi e^2/\hbar)t^2$, and agrees with the well-known Ambegaokar-Baratoff formula [9] at zero temperature.

Now we turn to the question what happens when the superconductors enter the regime $d \geq \Delta_{\text{BCS}}^2/\omega_{\text{Debye}}$, in which the BCS Ansatz wavefunction becomes inappropriate [5]. The transition to this regime is straightforward now, because the tight-binding model itself remains valid: The diagonal and off-diagonal matrix elements $E(\nu)$ and E_J^0 of the tight-binding Hamiltonian (14), defined in equations (17) and (15), will no longer be given by the BCS expression, but will have to be evaluated using the exact ground state wave function: The effect of the discrete level spacing on the diagonal elements $E(\nu)$, given by equation (17), will be to lift the degeneracy among them, thereby suppressing pair tunneling.

The off-diagonal elements E_J^0 will change with respect to their BCS value (18) due to several effects when the superconductors become small: (i) The excitation energies $E_{rl\nu}$ in equation (13) will include a term from the charging energy in the intermediate state, as studied in [15]. We neglect this effect, because we have chosen not to study charging effects at all. Furthermore, the change in superconducting correlations due to the finite level spacing will affect both (ii) the excitation energies E_r and E_l in equation (13) (which we, however, replace with their BCS value) and (iii) the matrix elements $\langle\nu|b_l b_r^\dagger|\nu+1\rangle$ that enter E_J^0. Finally, (iv) the shift of the Fermi level between the states $|\nu\rangle$ and $|\nu+1\rangle$ will also change the matrix elements E_J^0, as is explained in Section 4.1 below.

As it turns out (see Sect. 4.1 below), E_J^0 *increases* with increasing level spacing d, mainly due to the effect (iv). Once E_J^0 becomes comparable to $\Delta_{\rm sp}$, the lowest pair breaking ("single-particle") excitation energy, the superconductors can no longer be considered as weakly coupled, and the tight-binding model itself loses its validity.

2.5 The effect of charging energy

As mentioned in the introduction, the Coulomb charging energy plays an important role in small superconductors. Although we shall neglect it in the remainder of this paper, here we present a brief qualitative discussion of its main effects. The charging energy $E_C = (2e)^2/C$, C being the inter-grain capacitance, is the energy cost for tunneling an electron pair from one grain to the other. It introduces an additional term in (14), $E(\nu) = E_C(\nu-\nu_0)^2$. E_C can become huge in the small grain limit and essentially destroys the Josephson effect, since it suppresses pair tunneling.

Even if a gate is used to make two states $|\nu\rangle$ and $|\nu+1\rangle$ degenerate by a suitable choice of the gate voltage (i.e. $\nu_0 = 1/2$ plus an integer), such that at least one pair can still tunnel between the grains at no energy cost, the charging energy might nevertheless destroy the Josephson effect altogether: It may cause one electron pair to break into two unpaired electrons, one on each grain, if the associated lowering of the charging energy exceeds the energy necessary to form a pair-breaking excitation.

An order-of-magnitude estimate shows that this actually happens in the regime that the level spacing is important, if no measures are taken to reduce the charging energy: (i) As explained above, the charging energy must be smaller than the lowest energy of a pair breaking excitation, $E_C < \Delta_{\rm sp}$, such that no pair breaking excitations occur. (ii) $\Delta_{\rm BCS} < \sqrt{\omega_{\rm Debye}\, d}$ must be satisfied if the grains are to be small enough so that deviations from BCS become important (the 'weak' criterion in [5]). (iii) For the present purpose of constructing an order-of-magnitude estimate, we take $\Delta_{\rm sp} \sim \Delta_{\rm BCS}$, although these two energy scales may not be identical in the small-grain limit [5]. (They differ, for example, by a factor of up to two for the parameter range shown in Fig. 1 of [5].)

Putting (i) to (iii) together, the inequality

$$E_C < \sqrt{\omega_{\rm Debye}\, d}, \tag{20}$$

independent of λ, has to be satisfied.

Let us now explore what this implies for real aluminium grains: If the inter-grain capacitance is modelled by an aluminium oxide ($\epsilon \approx 8$) layer of thickness 15 Å and area πr^2, then $E_C \approx 0.8\ \mathrm{eV}(r/\mathrm{nm})^{-2}$. (A smaller thickness D in principle linearly decreases the charging energy, but at the same time, the inter-grain coupling t is exponentially increased [13], $t^2 \propto \exp[-D/(0.54\ \text{Å})]$. Since at a thickness of less than ∼15 Å, the grains are so strongly coupled that thay can no longer be considered as distinct, this distance seems to be a realistic order-of-magnitude lower bound for D.) Using the Debye energy $\omega_{\rm Debye} = 35$ meV for aluminum, we obtain $\sqrt{\omega_{\rm Debye} d} = 0.054\ \mathrm{eV}(r/\mathrm{nm})^{-3/2}$, and equation (20) implies $r > 250$ nm. At such a large size, aluminum is well in the BCS regime. According to criterion (ii) above, deviations from the BCS approach for a grain of that size would be observable only for a material with $\Delta_{\rm BCS} < 10^{-5}$ eV, an order of magnitude less than Al.

As an example, we consider the experiments of Nakamura et al. [16], which use a superconducting island with $\Delta \approx 230\ \mu$eV and $E_C \approx 117\ \mu$eV. These islands are evidently so small that they are quite close (up to a factor of 2) to the regime where the charging energy would begin to suppress pair tunneling by favoring single-particle excitations. Nevertheless, their islands are still large enough to be well described by BCS theory.

However, as mentioned in the introduction, the interest of this paper is to study the effects due to the discrete spacing of the energy levels, since the charging effects have already been discussed previously [11,12,15]. Therefore, we henceforth set the charging energy to zero.

2.6 Generalization to strong coupling

In the weak coupling limit, we have defined the Josephson energy via the part of the energy (8) that depends on φ. However, equation (8) is only valid for weak coupling (i.e. in second order in the single electron tunneling). We may equivalently define the Josephson energy as the maximally possible energy lowering due to coherent *pair* tunneling, i.e. when single electron terms are neglected as in the derivation of (13):

$$E_J \equiv E_{\rm coupled} - E_{\rm uncoupled}. \tag{21}$$

This definition agrees with the usual one (8) in the weak-coupling regime, because the maximally possible energy lowering occurs at phase difference $\varphi = 0$. Equation (21) allows an extrapolation to strong coupling as well, and therefore we will use it henceforth.

Unfortunately, the pair tunneling Hamiltonian (13), being only derived in second order perturbation theory, loses its validity for strong coupling; in general, one would have to use the single-electron tunneling Hamiltonian (10)

in that case. For simplicity, however, we choose for our strong coupling analysis a somewhat different coupling term that only includes pair tunneling,

$$H'_J = -\frac{\gamma d^2}{\Delta_{\rm BCS}} \sum_{rl} (b^\dagger_{1r} b_{2l} + \text{h.c.}), \tag{22}$$

and that differs from the pair tunneling Hamiltonian (13) in that the intermediate energy $E_r + E_l$ has been replaced by the constant $\Delta_{\rm BCS}$. Therefore, the Hamiltonian (22) and (13) are not equivalent. It is nevertheless interesting to study the Hamiltonian (22) for several reasons: Firstly, it captures the essential physics of the Josephson effect in a simple way: two superconductors coupled by a tunneling barrier that allows for pair tunneling. After all, it is the pair tunneling and not the single electron tunneling that is at the heart of the Josephson effect. Secondly, for $\gamma d/\Delta_{\rm BCS} = \lambda$, the total Hamiltonian looks just like one single superconductor, thus (22) is able to describe the transition to the strong-coupling regime where two superconductors effectively become one. Thirdly, it is amenable to a rather straightforward treatment by the DMRG approach (in contrast, H'_J of Eq. (13) would require much more numerical effort), which has the very significant advantage of yielding direct access to the regime of strong coupling between the two superconductors.

At weak coupling, a tight-binding analysis for (22) similar to the one that led to equation (18) can be performed. In the large grain limit, one finds the Josephson energy to be

$$E^0_J = \frac{2\gamma\Delta_{\rm BCS}}{\lambda^2}, \tag{23}$$

independent of d. In other words, the Hamiltonian (22) has a well-defined continuum limit when γ is held contant as $d \to 0$, as it should.

3 DMRG approach

In the context of nuclear physics, Richardson found an exact solution [4] of the Hamiltonian (9) for a single superconductor, that allows in principle to calculate all of its eigenenergies and eigenstates. Because the tight-binding calculation for weakly coupled superconductors, as outlined in Section 2.3, only needs the matrix elements (15) between states of a single superconductor, Richardson's solution is, in principle, sufficient for that case.

However, while the eigenenergies of (9) can be calculated with only little numerical effort using Richardson's solution, the computation time needed for the eigenstates and for matrix elements like the ones in (15) scales like $n!$ with the number of energy levels n in the system, making it effectively impossible to go beyond, say, $n = 12$ levels or so (more precisely, only the number n of energy levels between $E_{\rm Fermi} - \omega_{\rm Debye}$ and $E_{\rm Fermi} + \omega_{\rm Debye}$ matters). For this reason, despite there being an exact solution available, it is indispensable also for the tight-binding model to have an alternative approach at hand that is approximate, but manageable. Moreover, for the strong coupling analysis in Section 2.6, that invokes the pair tunneling term (22), Richardson's solution is not applicable at all, so that the use of a different approach becomes unavoidable.

For these reasons, we have adopted an approach based on the density matrix renormalization group (DMRG), whose power and efficiency for dealing with pair-correlated nanograins has been demonstrated recently [7,18]. We will use two kinds of DMRG calculations: A single-grain DMRG for calculating the matrix elements (Sect. 15) to be used in the tight-binding model at weak coupling (cf. Sect. 2.3), and a two-grain DMRG for the case of strong coupling (cf. Sect. 2.6).

In this section, we first discuss some general aspects of the DMRG algorithm in energy space in Section 3.1, leaving some of the more technical issues for Appendix A. In Section 3.2, we discuss the one-grain DMRG, and turn to the discussion of the two-grain DMRG in Section 3.3.

3.1 The DMRG method in energy space

The DMRG in its usual implementation is a real-space renormalization group method, and has been very successful for describing one dimensional many-particle quantum systems, such as spin chains [17]. Usually, the Hilbert space for such systems is too large to be diagonalized exactly on a computer. The DMRG algorithm allows to keep only a reduced part of the Hilbert space that is small enough to be tractable even on a desktop computer, but still sufficient to describe one or several desired states, the so-called target states (in our case, the ground state will be the target state). This is achieved by progressively increasing the chain size, adding sites one at a time, while only a limited number of states is kept at each step, those states being selected as the most relevant ones for describing the target state(s) in a density matrix analysis.

Although the DMRG is mostly limited to one dimensional systems, it can be applied to three dimensional ones by using the energy axis as the one dimensional "system", such that the bare energy levels play the role of sites on a one dimensional chain. This is not always useful, because the interactions between these "sites" can be much messier than between sites in real space, the latter being generally local. Luckily, as will be seen, the BCS interaction is, although nonlocal, simple enough for the DMRG algorithm to be applicable.

The DMRG builds up the system, starting from the low-lying energy states around the Fermi surface, which are the physically most important ones, and successively adds levels lying further and further away from the Fermi energy. It should be noted that this is quite contrary to the way usual RG calculations are performed, where high energy levels are integrated out, approaching the low energy states from above. This allows these two complementary approaches to be simultaneously applied: As long as not all energy levels have yet been added to the system, only the ones near the Fermi surface are explicitly included in the DMRG calculation. The other ones, which will be included only at later steps, are meanwhile taken into

account using a renormalization of coupling constants (as introduced in Eq. (43) of [18]).

For this purpose, the following scheme turns out to be numerically very efficient for renormalizing the coupling constants λ and γ: When the i levels closest to the Fermi energy are included, choose the coupling constants, say λ_i and γ_i, such that the BCS band gap Δ_i of the current system equals the final value Δ_n, where n is the desired final number of levels. In the DMRG for a single grain, $\Delta_i^{(1)} = id/(2\sinh(1/\lambda_i))$. In the two-grain DMRG, the band gap is given by $\Delta_i^{(2)} = id/\sinh(1/(\lambda_i + \gamma_i d/\Delta_n))$. The latter is the the solution of the BCS gap equation with two different interaction matrix elements $-\lambda_i d$ and $-\gamma_i d^2/\Delta_n^{(1)}$, as in (9) and (22). For large couplings, this scheme turns out to be more efficient than a perturbative renormalization of the coupling constants. At weak couplings, for which perturbation theory is expected to work, both approaches perform equally well.

Another drastic reduction of degrees of freedom occurs because in the model we study, the energy levels that are occupied by a single electron completely decouple from all the interaction terms (9), (13) and (22). Because the creation of a singly occupied level is associated with the energy Δ_{sp} and therefore energetically unfavorable, there will be no singly occupied levels in the low-energy sector of a superconductor, if one assumes the total number of electrons to be even. Due to these considerations, we can omit these levels from the beginning, and consider only the case of empty or doubly occupied energy levels [2].

Although the full Hilbert space is drastically reduced by the DMRG algorithm, it produces excellent results. In the case of the two-grain DMRG, the accuracy can be checked by comparing the condensation energy from DMRG to the Richardson solution, which is available for two specific values of the inter-grain coupling γ in (22), namely for [14] $\gamma d/\Delta = \lambda$ (which effectively describes one single, larger superconductor) and $\gamma = 0$ (two independent superconductors). The results for the two-grain DMRG are shown in Figure 1 and show the following features: (i) High precision at strong inter-grain coupling, with a relative error in the condensation energies of only $\sim 10^{-7}$ when $m = 100$ states are kept. (ii) Lower, but still sufficient precision for decoupled grains ($\gamma = 0$): $\sim 10^{-3}$ for $m = 300$, for $n = 100$ energy levels. However, the algorithm fails at weak coupling when the number of energy levels n becomes large ($N > 80 - 150$), see Section 3.3. In this case, a perturbative calculation (see Sect. 3.2) becomes necessary.

With the one-grain DMRG, the accuracy of case (i) is obtained. As always in DMRG, the precision can be systematically improved by increasing m.

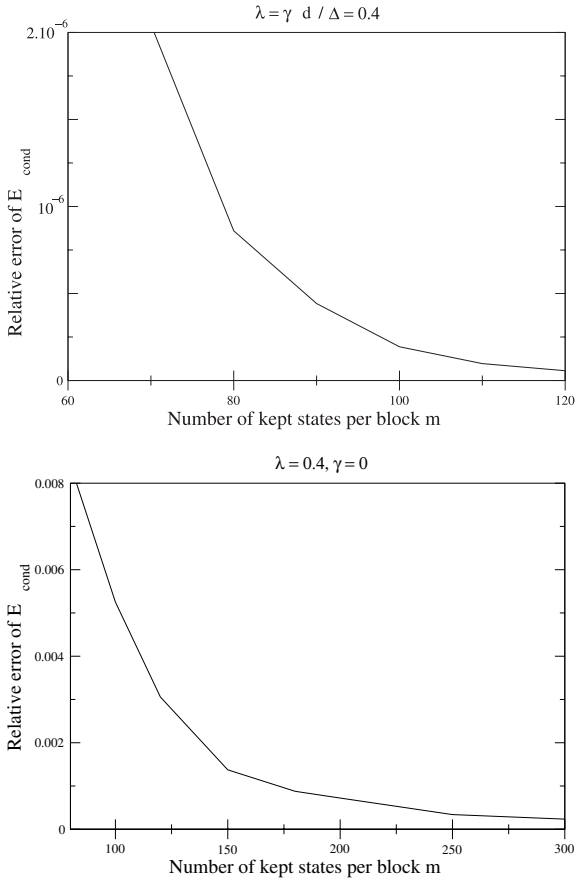

Fig. 1. Relative error between the exact result from Richardson's solution and the two-grain DMRG at BCS coupling $\lambda = 0.4$, with $n = 100$ energy levels per grain. The inter-grain coupling in the upper plot is $\gamma d/\Delta = \lambda$. In the lower plot, $\gamma = 0$.

3.2 One-grain DMRG for tight-binding model

If the grains are weakly coupled, the tight-binding approach can be applied, based on the Hamiltonian (13). Here, the microscopic model only enters via the tunneling matrix elements E_J^0 (15) of the tight-binding Hamiltonian (14). Although these can in principle be calculated exactly using Richardson's solution, in practice the DMRG algorithm is much better suited for that task, as explained above.

Assuming $\nu \ll N$ and using equation (5), the only matrix elements needed for E_J^0 are $\langle N/2+1|b_i^\dagger|N/2\rangle$ for all values of i. We evaluate these matrix elements using the DMRG algorithm for one single grain, as introduced in references [7,18]. This requires the simultaneous knowledge of two ground states with different pair occupation numbers, $|N/2\rangle$ and $|N/2+1\rangle$. These states are constructed in a single run, as explained in Appendix A. Once these matrix elements have been calculated, it is straightforward to diagonalize the tight-binding Hamiltonian (14).

3.3 Two-grain DMRG

If the DMRG is directly applied to a system of two grains, the regime of strong coupling can be explored, too. For this purpose, we use the inter-grain coupling term (22), introduced in Section 2.6. The exact Richardson solution cannot be applied for this system (except for the particular

value of $\gamma = \lambda d/\Delta_{\rm BCS}$, which has been used in Section 3.1 for checking the accuracy of the results).

Although the two-grain DMRG can cover the previously unaccessible parameter region of strong coupling, it turns out to fail for too weak inter-grain coupling, if the system is large (more than, say, 80−150 or so energy levels, depending on the other parameters). The reason is that the DMRG relies on correlations between the grains for being able to effectively reduce the Hilbert space, and these correlations vanish in the limit $\gamma \to 0$. This can easily be seen in the limiting case $\gamma = 0$, in which the two grains L and R are completely uncorrelated and can, each, be described by m_1 independent basis vectors $|1\rangle_L, ..., |m_1\rangle_L$ and $|1\rangle_R, ..., |m_1\rangle_R$. This implies that the m basis vectors retained are essentially product states of the form $|i\rangle_L \otimes |j\rangle_R$, and only an accuracy corresponding to $m_1 = \sqrt{m}$ kept basis vectors per grain is attained. If the inter-grain coupling γ is increased, correlations between grains L and R quickly develop that allow to keep only a few dominant ones of the product states, but for $\gamma = 0$, and also for very small values of γ, each of these states is equally important, making the DMRG highly inefficient. That the DMRG still works even for $\gamma = 0$ if only a few ($< 80-150$) energy levels are considered, is due to the fact that in this case, the necessary number of states to be kept per grain seems to be so low ($m_1 \approx 15$) that the ground state can still be reasonably well approximated.

To summarize, the two-grain DMRG works well for strongly correlated systems, but produces unsatisfying results for the case of weak inter-grain coupling. However, this is the regime in which perturbation theory can be used, as described before: thus, the two-grain DMRG and perturbation theory are two complementary approaches; their regimes of usefulness are illustrated in Figure 5 below.

4 Results

4.1 From small to large grains: The effect of discrete energy levels within the tight binding model

Figure 2 presents our results for the Josephson energy E_J, defined as the delocalization energy (21) due to pair tunneling, in the tight-binding approximation, calculated using the coupling Hamiltonian given by equation (14). E_J is plotted in units of the BCS result $E_J(BCS)$, given by equation (19). The dashed line in Figure 2 displays the Josephson energy as a function of decreasing level spacing d, i.e. of increasing grain size, characterized by the number of discrete energy levels n between $\varepsilon_F \pm \omega_{\rm Debye}$.

While the level spacing d is varied, the parameters λ and γ in (13) are held fixed (at the values $\lambda = 0.3$, $\gamma = 0.05$), such that the BCS value in equation (18) of E_J is independent of the grain size, and a well-defined limit $d \to 0$ exists.

Within the tight-binding model, we observe two competing effects, to be discussed in detail below, that influence the Josephson energy as the level spacing d increases

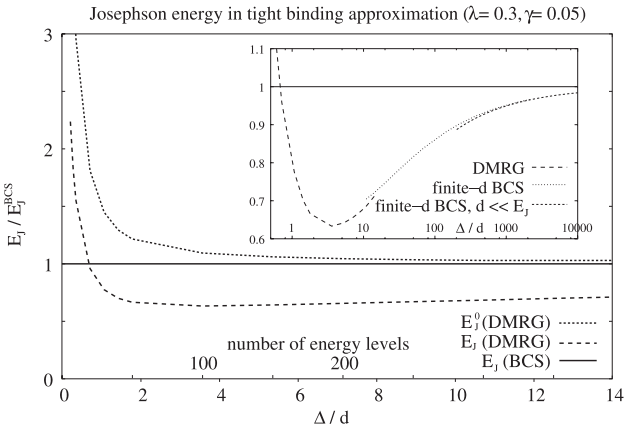

Fig. 2. The Josephson energy E_J in the tight-binding approximation, based on equation (14), as a function of the grain size. E_J is defined via equation (21) as the additional energy gain due to coherent pair tunneling and is normalized to the BCS result $E_J^{\rm BCS}$ in equation (19). Compared to the off-diagonal matrix element E_J^0 (dotted line), E_J (dashed line) is reduced by a factor of up to 2 due to the finite-size kinetic energy term $E(\nu)$ of equation (17). The logarithmic plot in the inset shows how the BCS result of equation (19) is recovered as $d \to 0$.

(i.e. moving toward the left side of Fig. 2): (i) On the one hand, the finite-size kinetic energy term $E(\nu)$ of equation (17) increases, which tends to reduce the Josephson energy E_J; (ii) on the other hand, the off-diagonal matrix element E_J^0 in equation (14) increases (as shown in Fig. 2, dotted line), which tends to increase E_J. The combination of these two tendencies leads to the reentrant behaviour seen in Figure 2, particularly in the inset, with a remarkable *increase* in E_J when d becomes sufficiently large.

The kinetic term (i) was discussed in Section 2.3. We chose ν_0 in equation (17) as $\nu_0 = 1/2$, such that the two lowest-lying states are degenerate and at least one pair can tunnel at no energy cost between these states no matter how large d is. For this case, the total reduction of the Josephson energy due to the finite-size kinetic term amounts to a factor of at most 2, even for very large level spacing d. This is because for $d \to \infty$, all but the lowest two states "freeze out", so that the tight-binding Hamiltonian (14) effectively reduces to a two-level system for the states $|\nu = 0\rangle$ and $|\nu = 1\rangle$, whose tunnel splitting is $E_J^0/2$ (hence the reduction by a factor of 2). Nevertheless, the reduction in Figure 2 is seen to be considerable even for fairly large grains (still of order 20 % for $\Delta_{\rm BCS}/d \sim 100$, corresponding to $n \sim 3000$ levels), because it depends on the ratio d/E_J^0, where E_J^0 typically is a small number itself. For $d \ll E_J$, the asymptotic behaviour $E_J = E_J^0(1 - \sqrt{2d/E_J^0})$ (thin dashed line in the inset of Fig. 2) is found in analogy to the treatment of small charging energies in Section 7.3 of [19], by using an Ansatz wave function given by equation (4) with $\varphi = 0$ and C_ν of Gaussian form. This Ansatz wave function turns out to be asymptotically correct for $d \ll E_J^0$ [19].

Next, we discuss the increase of E_J^0 in the small-grain limit (ii). It is due to the fact that the matrix elements

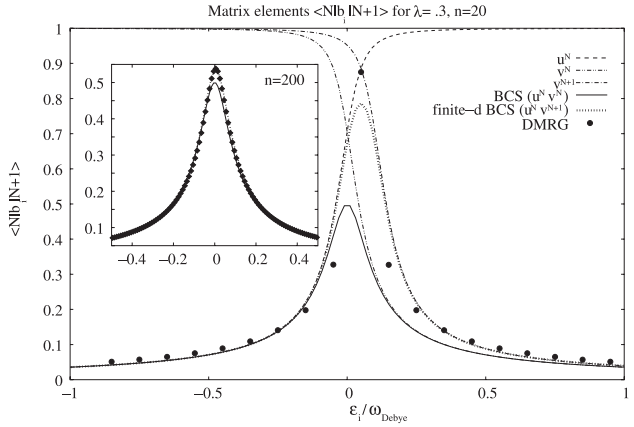

Fig. 3. Various approximations for the matrix element $\langle N|b_i|N+1\rangle$ are compared. The product of the BCS coherence factors $u^N v^N$ (BCS, thin dashed line) is compared to $u^N v^{N+1}$ (finite-d BCS, solid line) in a grain of $n = 20$ levels. Because v^{N+1} in the latter product is shifted to the right by an amount of d with respect to v^N, the finite-d curve must obviously be larger than the BCS curve for all values of i. Also shown (filled dots) are the exact matrix elements $\langle N|b_i|N+1\rangle$, calculated using the DMRG approach. The inset compares the BCS, the finite-d BCS and the DMRG results for a larger grain with $n = 200$ levels. While the finite-d BCS result shows excellent agreement with the DMRG result in this regime, the BCS result still deviates from the exact result.

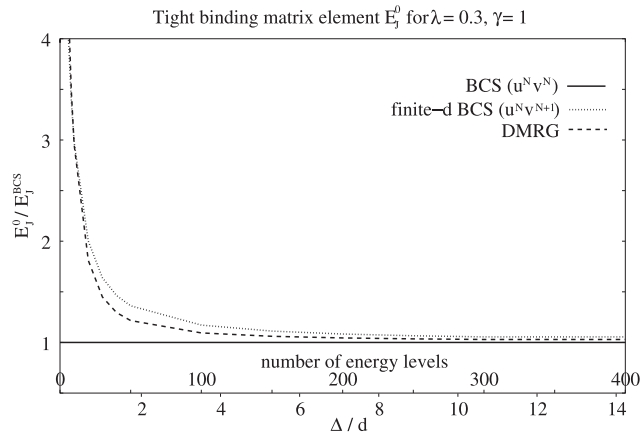

Fig. 4. E_J^0 is evaluated in the BCS, the finite-d BCS and the DMRG method. Although BCS theory is not valid in the regime of large level spacings d, the finite-d-BCS reproduces, at least qualitatively, the correct behaviour seen in the DMRG curve.

$\langle N_L|b_l|N_L+1\rangle\langle N_R+1|b_r^\dagger|N_R\rangle$ that contribute to E_J^0 in equation (15) have a different number of electron pairs in the states acting from the left and on the right. This fact is neglected in standard BCS theory, where the total number of pairs is assumed to be macroscopically large anyway. When the level spacing d becomes large, however, this is the main reason for the increase of E_J^0.

The increase of E_J^0 is easy to understand for the Fermi state ($\lambda = 0$) and in the BCS limit ($\lambda > 2/\ln N$, see [5]). In the Fermi state, the matrix element $\langle N|b_i|N\rangle$ is zero for all values of i, but $\langle N|b_i|N+1\rangle$ gives a contribution of 1 for the one level $i = i_N$ that is below the Fermi surface of $|N+1\rangle$ and above the Fermi surface of $|N\rangle$. In the BCS case, the matrix element is given by $\langle N|b_i|N+1\rangle = u_i^N v_i^{N+1}$. The upper indices on u and v indicate the total pair occupation numbers with respect to which they are taken, with the effect that v^{N+1} (dashed-dotted line in Fig. 3) has the chemical potential shifted upwards with respect to v^N (dashed-double-dotted line) by the level spacing d, and hence is shifted to the right in Figure 3 by this amount. Thus, the product $u_i^N v_i^{N+1}$ becomes larger as the level spacing d increases, as is illustrated in Figure 3. We shall call this modification of the BCS calculation the "finite-d" BCS calculation.

In Figure 3, the finite-d BCS matrix elements (solid line) are also compared to the exact values obtained using the DMRG (filled dots). The comparison shows that for the levels close to the Fermi energy (i.e. the central level i_N and the next, say, 2 levels), the finite-d BCS result overestimates the pairing correlations: the (quasi-) exact DMRG solution is seen to have a more pronounced peak at the central level i_N, whereas the contribution of the neighbouring two levels is somewhat reduced, resembling, for these levels, qualitatively more closely the $\lambda = 0$ case discussed above. For the energy levels further away from the Fermi energy than that, the finite-d BCS calculation is seen to slightly underestimate the matrix elements. This is not unexpected, because BCS theory is known [5] to underestimate the superconducting correlations of energy levels much farther away from the Fermi surface than $\Delta_{\rm BCS}$, which for the parameters of Figure 3 is $\Delta_{\rm BCS} \approx 0.7$.

E_J^0, however, being a weighted sum over all products of these matrix elements, is nevertheless not so far off in the finite-d BCS approach even for very small grains, as can be seen in Figure 4. This is surprising and somewhat fortituous, since the BCS theory does not self-consistently describe the grains in the limit that they are small. The reason that the finite-d BCS works so well seems to be that the underestimation of the matrix elements for level i_N and and their overestimation for the other levels cancel each other to a large degree.

In conclusion, the main reason why E_J^0 increases as the grains become small is very simple: the chemical potential of the grains shifts due to the finite level spacing whenever a pair tunnels from one grain to the other. Note that the BCS ansatz without taking this effect into account is not accurate near the Fermi energy even for fairly large grains (see the inset in Fig. 3), for which the finite-d BCS theory agrees perfectly with the DMRG result.

The competition between the finite-size kinetic term on the one hand and the increase of E_J^0 on the other leads to the reentrant behaviour of E_J as seen in Figure 2. This is one of our main results. Two regimes can be distinguished as a function of $\Delta_{\rm BCS}/d$: For very small grains ($\Delta_{\rm BCS}/d < 1$), superconducting correlations are only weakly present, but the 1-level effect outlined above leads to a strong enhancement of E_J^0 and, therefore, of the Josephson energy E_J. Despite not being a well-justified

approximation in this regime, the finite-d BCS result nevertheless gives a surprisingly good estimate of the Josephson energy. On the other hand, for larger values of $\Delta_{\rm BCS}/d$ (>10, say), E_J^0 is almost constant and very close to the BCS value. The kinetic energy term in equation (17), however, reduces the Josephson energy below the BCS value, and vanishes only rather slowly. The reentrant behaviour of E_J occurs at the intermediate region $1 < \Delta_{\rm BCS}/d < 10$, in which both effects are competing, and in which E_J^0 is slowly approaching its BCS value from above.

In the above discussion, the Coulomb charging energy E_C was neglected (see Sect. 2.5). As long as $E_J < E_C < \Delta_{\rm sp}$, E_C can actually be included in the tight-binding model without much effort [12,19]; the only modification is in the Hamiltonian of equation (17), where d has to be replaced by $d_{\rm eff} = d + E_C > E_J$. Thus, the only consequence of charging energy is that the description in terms of an effective two-level model with states $|\nu\rangle$ and $|\nu+1\rangle$, given above for $d \to \infty$, must now be applied for all values of d (as long as one still restricts the discussion to the degeneracy point, where $\nu_0 = 1/2$). In particular, the estimate $E_J = E_J^0/2$ holds for all values of d, with E_J^0 as shown e.g. in Figure 2. Therefore, the increase of E_J shown in the small-grain limit ($d \to \infty$) of Figure 2 is present also for $E_C > 0$. The reentrant behaviour as $d \to 0$, however, is no longer seen; instead, E_J saturates at the value $E_J^{\rm BCS}/2$. On the other hand, if $E_C > \Delta_{\rm sp}$, the tight-binding model itself is no longer a good starting point. This case was discussed in Section 2.5.

4.2 Limitations of the tight-binding approach

The tight-binding approximation, which neglects pair breaking excitations of the individual grains, is valid only for small couplings, such that E_J^0 lies well below the lowest excitation energy $\Delta_{\rm sp}$. In Figure 2, however, E_J^0 is seen to grow strongly with increasing level spacing d. Thus, for sufficiently large d, the tight-binding approach invariably becomes unreliable, and a different method is needed. In order to complement the tight-binding approach and to check its quality, we have thus used the two-grain DMRG solution that does not rely on the inter-grain coupling being weak.

The DMRG, however, has its own limitations, as was explained in Section 3.3: Firstly, it requires a pair tunneling Hamiltonian (22) that describes a somewhat different model. This implies, of course, that it has to be compared to a tight-binding model using the same pair tunneling Hamiltonian as well. Secondly, the two-grain DMRG can break down at small couplings if the number of energy levels is large, for precisely the same reason that the tight-binding model works well: The correlations between the two grains, which the DMRG relies on, become very weak.

The regimes of validity of the two complementary approaches are schematically depicted in Figure 5. The tight-binding method only works well at small coupling, $\Delta_{\rm s.p.} \ll E_J$ (region left of dashed line), whereas the DMRG works well only at large coupling (region right of solid line). A simple (analytical) condition for the validity

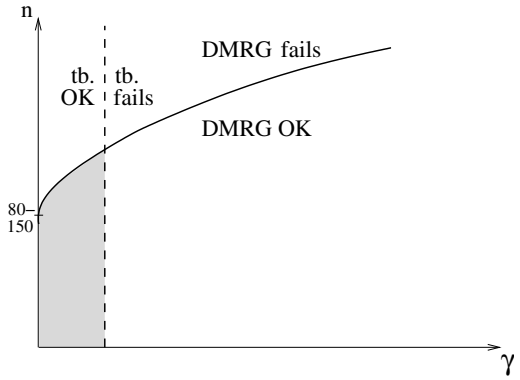

Fig. 5. A rough sketch of the regimes of validity for the DMRG and the tight-binding approach in parameter space (inter-grain coupling γ vs. the number n of energy levels). There is only a small overlap (shaded region) at small γ and small n, in which both approaches simultaneously work well.

of the DMRG approach cannot be given, which is why the axes in Figure 5 are drawn without units. However, the quality of the DMRG approach is found to depend sensitively on the number of energy levels n. In particular, the DMRG turns out to be reasonably accurate for all values of γ down to 0, as long as $n < 80{-}150$ (depending on other parameters), as is motivated in Section 3.3 and seen in Figures 6 and 7.

In Figures 6 and 7, the tight-binding approximation for the Josephson energy is compared to the two-grain DMRG as a function of the grain size, for two different values of the inter-grain coupling γ (corresponding to moving along vertical lines in Fig. 5). The Josephson energies are again plotted in units of their BCS values, now given by equation (23). In Figure 6, both methods are seen to agree for small numbers of energy levels, $n < 80{-}100$. For larger values of n, the two-grain DMRG breaks down, for the reasons outlined in Section 3.3. The DMRG method itself signals its own breakdown: Convergence as function of the kept DMRG states m is no longer achieved, as can already be seen when the two curves shown in Figure 6, which correspond to $m = 330$ and $m = 360$, are compared.

Since both the two-grain DMRG and the tight-binding approach are ultimately variational methods, the one that produces the higher value of E_J (i.e. the lower total condensation energy) must be the better approximation. Also in this respect, the DMRG method is seen to be failing for $n > 80 - 100$ in Figure 6, in agreement with Figure 5.

Figure 7 shows the result of a similar calculation as Figure 6, at a higher value of the inter-grain coupling $\gamma = 0.01$. Now, the two-grain DMRG is seen to be valid up to somewhat larger values of n. For small n, $n < 100$, the DMRG now produces a higher value of E_J, indicating that in this regime, it produces a better result than the tight-binding method, as anticipated in Figure 5.

The results from Figures 6 and 7 are similar to the ones in Figure 2, where only a tight-binding calculation had been performed. In particular, the two-grain DMRG reproduces the increase in E_J for small values of n, corresponding to large level spacing d, and thereby confirms

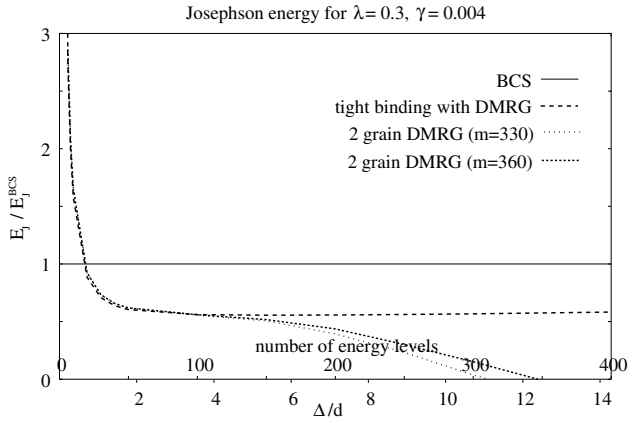

Fig. 6. The Josephson energy is calculated in the tight-binding and in the DMRG approach. In agreement with Figure 5, both curves agree if the number of energy levels n is small, but the DMRG fails for $n > 80-100$.

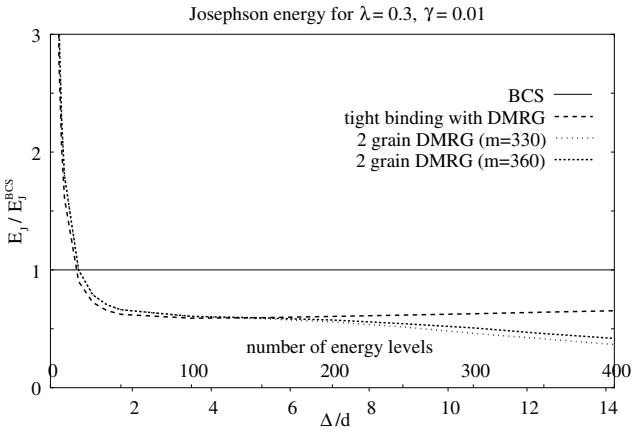

Fig. 7. Same calculation as in Figure 6, but at larger inter-grain coupling. Now, the DMRG has a somewhat larger range of validity. For small grains, the DMRG curve lies higher (i.e. the tight-binding approach is not as good as the DMRG anymore).

the reentrant behaviour observed in the tight-binding approach (cf. Fig. 2).

In Figure 8, the tight-binding and the two-grain DMRG results are plotted as a function of the inter-grain coupling γ (corresponding to moving horizontally in Fig. 5). The plot is extended to very large values of the inter-grain coupling γ in order to show the point at which the two-grain DMRG can be compared to the exact result at $(d/\Delta_{\rm BCS})\gamma = \lambda$, which it reproduces nicely. We emphasize that in the regime of large γ, some of the physical assumptions (e.g. the use of a tunneling Hamiltonian) of our calculation are not justified anymore, and that the plot in that regime has no other physical significance than to provide an important cross check for the DMRG.

The exact result at $(d/\Delta_{\rm BCS})\gamma = \lambda$ describes the two grains as a single superconductor with half the level spacing $d_2 = d/2$ and with the interaction Hamiltonian

$$H_2 = -\lambda_2 d_2 \sum_{i\in R,L,\ j\in R,L} b_i^\dagger b_j, \qquad (24)$$

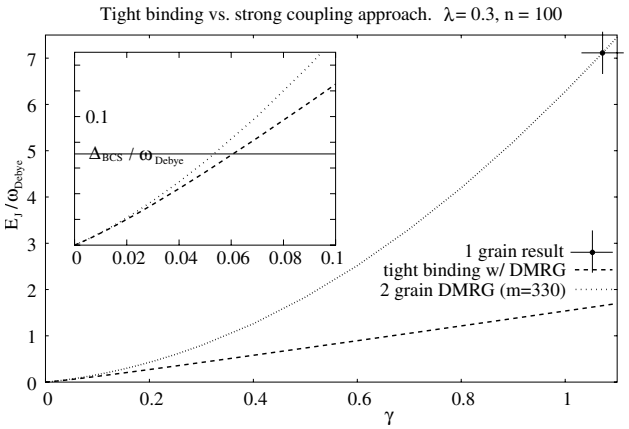

Fig. 8. The Josephson energy is plotted as a function of the inter-grain coupling γ in grains that are small enough so that the DMRG approach works for all values of γ down to zero. Once the coupling is too large ($\gamma \gtrsim 0.06$), the tight-binding model fails as asserted in Figure 5. The inset shows an enlargement for small values of γ, and illustrates the condition $E_J \ll \Delta_{\rm sp} \sim \Delta_{\rm BCS}$ for the tight-binding model to be valid, which was motivated at the beginning of Section 2.

.

and with $\lambda_2 = 2\lambda$. In the large-coupling regime, the Josephson energy $E_J = E_{\rm cond,2} - 2E_{\rm cond,1}$ is entirely dominated by the condensation energy $E_{\rm cond,2}$ of the large superconductor described by equation (24), which is much larger than the condensation energies $2E_{\rm cond,1}$ of the isolated grains (i.e. for $\gamma = 0$). In the BCS limit, $E_J \approx E_{\rm cond,2} = \omega_{\rm Debye} n \sinh^2(1/\lambda_2)$. In particular, E_J is seen to be an extensive quantity, i.e. $E_J/\omega_{\rm Debye} \propto n$ for the particular choice $\gamma = (\Delta_{\rm BCS}/d)\lambda$, for which the two superconductors are described as one. In this case the inter-grain coupling acts like a bulk term (and no longer as a surface effect), which is manifest in the way that γ scales with the system size: γ scales no longer as a constant, but with the volume of the system.

As is evident from Figure 8, the tight-binding method, which is only applicable at very small values of γ, ceases to be valid long before the point $(d/\Delta_{\rm BCS})\gamma = \lambda$ is reached. The inset of Figure 8 shows an enlargement of the main figure for small γ. It is seen that for $E_J^0 \ll \Delta_{\rm BCS}$, the results from the tight-binding method and from the DMRG agree, as expected.

This work was supported by the DFG Program "Semiconductor and Metallic Clusters". US and DG acknowledge support through a Gerhard Hess prize of the Deutsche Forschungsgemeinschaft. We thank G. Falci, Y. Imry, S. Kleff, C. Kollath, M. Schechter, and G. Sierra for discussions.

Appendix A: The DMRG algorithm in energy space

In this appendix, some technical aspects of the DMRG procedure for approximating the ground state $|\psi\rangle$ are explained. There are excellent pedagogical reviews of the

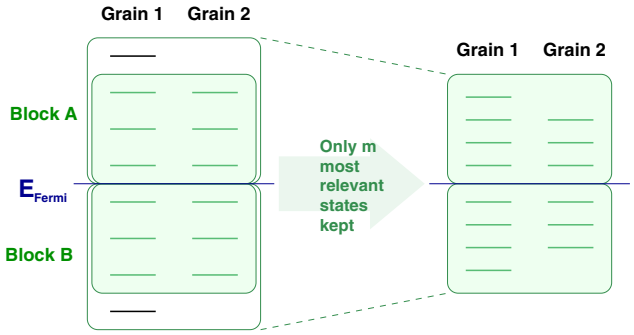

Fig. 9. Sketch of the procedure for projecting out the relevant states in the case of the two-grain DMRG. The shading indicates the part of the Hilbert space where only a limited number of states are kept. First, a new level is added on grain 1 (left part of figure). Then, the m most relevant states are projected out and kept (right part). Then, a new level on grain 2 is added (not shown).

DMRG algorithm to be found [17,20], as well as a description of its application to superconducting grains [7,18], so we only highlight the key concepts of the DMRG algorithm for reducing the Hilbert space. Then, the full DMRG algorithm as applied in energy space is sketched. Finally, a few peculiarities are mentioned that are of relevance when the algorithm is applied to the problem of two coupled superconductors.

First, we will give an account of the procedure that projects out a reduced number of basis states. The Hilbert space is divided into two blocks A of states below and B of states above the Fermi surface, as depicted in Figure 9, each being represented by the respective basis state $|i\rangle_A$ and $|j\rangle_B$. A general many-body state is expressed as $\sum_{ij}\psi_{ij}|i\rangle_A \otimes |j\rangle_B$. The goal is to find a reduced number m of most relevant states $|u_\alpha\rangle_A$ and $|u_\beta\rangle_B$, in the sense that they allow for the best approximation of the state $|\psi\rangle$, such that the norm $\left||\psi\rangle - \sum_{ij}\psi_{\alpha\beta}|u_\alpha\rangle_A \otimes |u_\beta\rangle_B\right|$ is minimized, when variation over both $\psi_{\alpha\beta}$ and the states $|u_\alpha\rangle_A$, $|u_\beta\rangle_B$ are allowed, but only m states per block are to be kept. It turns out that the states with this property are precisely those eigenstates of the reduced density matrix of the respective block (A or B) that correspond to the m largest eigenvalues [20]. Of course, the larger m is, the more accurate the algorithm becomes, until convergence is achieved. Typical values for m are $m \sim 100{-}400$.

The prescription for the DMRG algorithm is the following: (i) Start with only a few (2 or 3, say) energy levels, few enough that the exact basis of the many-body system can be kept explicitly. (ii) Add an additional energy level to block A and B, as depicted in Figure 9 for the case of the two-grain DMRG. Construct a basis $|u_\alpha\rangle_A$ for block A, using the basis states from the previous step and the exact basis of the newly added energy level. Do the same with block B. (iii) Calculate the target state $|\psi\rangle$, in our case the ground state of the BCS Hamiltonian, within the present Hilbert space. (iv) Calculate the reduced density matrix of $|\psi\rangle$ for block A and B, say ρ_A and ρ_B, by tracing out the full density matrix $|\psi\rangle\langle\psi|$ over the respective other block. Find the m eigenvectors $|u_\alpha\rangle_A$, $|u_\beta\rangle_B$, $\alpha,\beta = 1...m$, corresponding to the m largest eigenvalues of ρ_A and ρ_B. Those are the states to be kept as basis states. (v) Transform all operators to the new basis. If the blocks A and B are related by a symmetry, it may be sufficient to calculate only one set of states $|u_\alpha\rangle$. Continue with step (ii) and iterate, until the final number of energy levels is reached.

In step (iii), the ground state $|\psi\rangle$ is found using the Lanczos procedure, which is very efficient due to the sparse nature of the Hamiltonian, but which requires many multiplications of a state with the Hamiltonian. Since the Hamiltonian is a sparse but extremely large matrix (of order $m^2 \times m^2$), it is essential not to store it as a whole, but to reconstruct it from simple operators acting only on the blocks A and B when the multiplication is performed. For this to be numerically possible, it is necessary that the interactions between the blocks factorize to a large degree, such that they can be expressed as a sum of only a few terms. In real-space DMRG, this is always the case as long as the interactions are more or less local, but the long-range interactions in energy space do not always factorize. Luckily, the reduced BCS interaction does factorize nicely: $H_{BCS} = -\lambda(B_A^\dagger B_A + B_A^\dagger B_B + A \leftrightarrow B)$, where $B_{A,B} = \sum_{i\in A,B} c_{i\uparrow}c_{i\downarrow}$. A similar factorization is possible for the inter-grain coupling (22) in the two-grain DMRG, but not for (13).

It is also essential for numerical efficiency to make use of conserved quantum numbers. In our case, due to particle number conservation, it is not necessary to keep all the m^2 states $|u_\alpha\rangle_A \otimes |u_\beta\rangle_B$ as a basis. In our algorithm, we keep track of the number l_α, l_β of particle or hole excitations associated with each basis vector $|u_\alpha\rangle_A, |u_\beta\rangle_B$, respectively. Then, only the states $|u_\alpha\rangle_A \otimes |u_\beta\rangle_B$ have to be kept for which

$$l_\alpha - l_\beta = l_{\rm tot}, \tag{25}$$

where $l_{\rm tot}$ is the deviation of the total electron pair number from half filling.

In the tight-binding calculation, taking the matrix element $\langle n|b_i|n+1\rangle$ involves approximating two states simultaneously, namely the ground states $|n\rangle$ and $|n+1\rangle$ that correspond to the respective number of electron pairs n and $n+1$. This is simply done by calculating both states in step (iii), and by taking the reduced density matrix of the mixed state with equal weight in step (iv).

In the two-grain DMRG, the calculations are performed in the regime that two states, $|\nu\rangle$ and $|\nu+1\rangle$, as defined in equation (5), are degenerate. This is done by setting the offset between the energy levels on the left and the right grain to zero, and by including one more electron pair than there would be at half filling, which amounts to setting $l_{\rm tot} = 1$ in equation (25). This extra pair can, then, be on the left or the right grain at equal energy cost.

One complication arises away from half filling (i.e. when $l_{\rm tot} \neq 0$): When, in step (iv), the reduced basis of one block (block A, say) is calculated by tracing over the states in the other block, the part of the trace relevant for the

states with quantum number l_α is, due to equation (25), performed over states which carry a different quantum number l_β. The dimensionality of the two subspaces $\mathcal{H}(l_\alpha)$ and $\mathcal{H}(l_\beta)$ spanned by the part of the reduced density matrix with the respective quantum numbers might be quite different. However, the rank of the reduced density matrix used in step (iv) is limited by the dimension of the space over which the trace is performed, and therefore, the DMRG only works well as long as the dimension of $\mathcal{H}(l_\beta)$ is larger than the number of states with quantum number l_α to be kept. This is not guaranteed away from half filling, i.e. when $l_\alpha \neq l_\beta$.

The problem is solved by mixing a small part (20%) into the reduced density matrix that corresponds to the ground state at half filling ($l_{\mathrm{tot}} = 0$). This state will have a similar information content as the target state away from half filling, as far as the relevant basis vectors are concerned, and adds enough to the rank of the reduced density matrix for the DMRG to work well.

In the two-grain DMRG, the energy levels are added one by one as depicted in Figure 9: First levels on grain 1, and only afterwards levels on grain 2 are added. They are added one by one in order to keep the Hilbert space as small as possible. It is also possible and, in fact, would be more symmetric, to add both levels at once, but only at the cost of having the Hilbert space larger by a factor of 4. As it turns out, it is numerically more efficient (yielding higher accuracy at the same computation time) to add the levels one by one.

References

1. P.W. Anderson, J. Phys. Chem. Solids **11**, 28 (1959)
2. J. von Delft, D.C. Ralph, Phys. Rep. **345**, 61 (2001)
3. C. Black, D. Ralph, M. Tinkham, Phys. Rev. Lett. **76**, 688 (1996)
4. R. Richardson, N. Sherman, Nucl. Phys. **52**, 221 (1964)
5. M. Schechter, Y. Imry, Y. Levinson, J. von Delft, Phys. Rev. B **63**, 214518 (2001)
6. P.-G. de Gennes, *Superconductivity of metals and alloys* (Perseus books, 1999)
7. J. Dukelsky, G. Sierra, Phys. Rev. Lett. **83**, 172 (1999)
8. R. Ferrell, Phys. Rev. B **38**, 4984 (1988)
9. V. Ambegaokar, A. Baratoff, Phys. Rev. Lett. **10**, 486 (1963)
10. W. Hofstetter, J. Cirac, P. Zoller, E. Demler, M. Lukin, Phys. Rev. Lett. **89**, 220407 (2002)
11. D. Averin, K. Likharev, *Single electronics: A correlated transfer of single electrons and cooper pairs in systems of small tunnel junctions*, in *Mesoscopic phenomena in solids*, edited by B. Altshuler, P. Lee, R. Webb (Elsevier, 1999)
12. M. Iansiti, M. Tinkham, A. Johnson, W. Smith, C. Lobb, Phys. Rev. B **39**, 6465 (1989)
13. K. Knorr, J. Leslie, Solid State Commun. **12**, 615 (1973)
14. J. Links, K. Hibberd, Int. J. Mod. Phys. B **16**, 2009 (2002)
15. K. Matveev, M. Gisselfält, L. Glazman, M. Jonson, R. Shekhter, Phys. Rev. Lett. **70**, 2940 (1993)
16. Y. Nakamura, Y. Pashkin, J. Tsai, Nature **398**, 786 (1999)
17. I. Peschel, *Density matrix renormalization: a new numerical method in physics* (Springer, 1999)
18. G. Sierra, J. Dukelsky, Phys. Rev. B **61**, 12302 (2000)
19. M. Tinkham, *Introduction to superconductivity* (McGraw-Hill, 1996)
20. S.R. White, R.M. Noack, *Density matrix renormalization group*, in *Density matrix renormalization: a new numerical method in physics*, edited by I. Peschel (Springer, 1999)
21. In general, b_i annihilates a pair of electrons $c_{i\uparrow}c_{\bar{i}\downarrow}$ in time-reversed states $|i,\uparrow\rangle$ and $|\bar{i},\downarrow\rangle$; for the present context of nanograins in the absence of a magnetic field, however, we may take $i = \bar{i}$